arXiv:1601.02846v2 [cond-mat.stat-mech] 21 Apr 2016

Underlying mechanisms for normal heat transport in one-dimensional anharmonic oscillator systems with a double-well interparticle interaction

Daxing Xiong‡

Department of Physics, Fuzhou University, Fuzhou 350108, People's Republic of China

E-mail: phyxiongdx@fzu.edu.cn

Abstract. Previous studies have suggested a crossover from superdiffusive to normal heat transport in one-dimensional (1D) anharmonic oscillator systems with a double-well type interatomic interaction like $V(\xi) = -\xi^2/2 + \xi^4/4$, when the system temperature is varied. In order to better understand this unusual manner of thermal transport, here we perform a direct dynamics simulation to examine how the spreading processes of the three physical quantities, i.e., the heat, the total energy and the momentum, would depend on temperature. We find three main points that are worth noting: (i) The crossover from superdiffusive to normal heat transport is well verified from a new perspective of heat spread; (ii) The spreading of the total energy is found to be very distinct from heat diffusion, especially that under some temperature regimes, energy is strongly localized, while heat can be superdiffusive. So one should take care to derive a general connection between the heat conduction and energy diffusion; (iii) In a narrow range of temperatures, the spreading of momentum implies clear unusual non-ballistic behaviors; however, such unusual transport of momentum cannot be directly related to the normal transport of heat. An analysis of phonons spectra suggests that one should also take the effects of phonons softening into account. All of these results may provide insights into establishing the connection between the macroscopic heat transport and the underlying dynamics in 1D systems.

PACS numbers: 05.60.-k, 44.10.+i

‡ Author to whom any correspondence should be addressed.

1. Introduction

The viewpoint of anomalous heat transport in one-dimensional (1D) momentum-conserving systems has now been widely accepted [1, 2]. The anomaly means that the "standard" heat transport law, i.e., the Fourier's law of heat conduction, stating that, the heat flux $\boldsymbol{J}$ is proportional to the temperature gradient ∇T: $\boldsymbol{J} = -\kappa \nabla T$, with κ the heat conductivity assumed to be constant, is not validated. In particular, for 1D anharmonic oscillator systems with conserved momentum and symmetric interparticle interactions, it has now been generally believed that κ is not a constant but follows a simple space L scaling $\kappa \sim L^{\alpha}$ [1, 2]. (For the momentum-conserving systems with asymmetric interactions, refer to the recent progress [3, 4] and debates [5, 6, 7, 8]). Despite that there is still no consensus on the universality classes of the scaling exponent α and its accurate value(s), in most cases $0 < \alpha < 1$ [9, 10, 11, 12, 13, 14, 15, 16] can be concluded. This power-law space scaling has also been corroborated by some relevant experimental studies of carbon nanotubes [17].

Nevertheless, there are still at least two exceptional systems with both conserved momentum and symmetric interactions against the above belief [18], i.e., the 1D coupled rotator system and the chain with a double-well (DW) potential. For both systems a transition (or crossover) from superdiffusive to normal heat transport (obeys the Fourier's law, $\alpha = 0$) has been claimed to take place. Several mechanisms have been proposed to understand the observed normal transport in rotator systems. Early works related the mechanism to the occurrence of phase jump [19] and the excitation of high-frequency stationary localized rotational modes [20]. While quite recently the mechanism has been traced back to the diffusive behavior of the momentum spread [21] and the absence of the conserved quantity of stretch from the perspective of nonlinear fluctuating hydrodynamics [22, 23]. However, when one turns to the system with DW potential, the underlying mechanism for normal heat transport has not yet been clarified so far. Even worse, whether the transport would be normal or abnormal remains controversial: early results indicated that heat conduction is normal at low temperatures [19], nevertheless it was doubted later by [1, 2]. Two recent works revisited the issue and suggested that normal behavior may appear in a narrow temperature region near $T \simeq 0.1$ [24]. In a quite recent work, we have also shown convincing evidences for this normal behavior [25], however, the underlying mechanisms are still not very clear.

In the present work we perform a further careful simulation to examine the unusual heat transport and its underlying mechanisms in the 1D oscillator systems with DW potential. For such purpose we first consider the heat spreading process. To identify whether heat transport is normal or anomalous, usually the space scaling dynamical exponent α has been given the most efforts, for which two kinds of dynamics simulation approaches, i.e., direct nonequilibrium molecular dynamics simulations [26] and the method based on Green-Kubo formula [27], have been frequently used. However, just as raised by S. Olla [28] in a discussion session of a recent workshop: these studies for deriving α usually ignored another key time scale. Therefore, by viewing that

concerning the time scaling may involve more detailed information, which would enable us to present a more detailed prediction for heat transport, here we shall investigate the relaxation of equilibrium heat fluctuations of the system to derive the space-time scaling properties to characterize the heat transport behavior. We shall explore how this space-time scaling depends on system temperature, through which we are able to verify with satisfactory precision that, normal transport is indeed likely to take place near the crossover temperature $T \simeq 0.1$.

To further understand this normal transport of heat, we shall also investigate the relaxation of two other physical quantities fluctuations, i.e., the total energy and the momentum. We will show clear distinctions between the spreading of heat and the total energy. In some temperature regimes, we will also reveal the unusual non-ballistic behaviors of momentum spread. Nevertheless, the latter features of momentum spread cannot be directly attributed to the observed normal transport of heat. A careful analysis of the system's phonons spectra indicates that, around the crossover temperature point, phonons clearly tend to become softest. Based on both facts, we thus conjecture that under the appropriate temperature, phonons softening, together with the non-ballistic behavior of momentum diffusion, may result in the observed normal heat transport in the systems with DW potential.

2. Model

The considered model is a 1D momentum-conserving oscillator system with Hamiltonian of the form

$$H = \sum_k \left[\frac{p_i^2}{2\mu} + V\left(q_{k+1} - q_k\right) \right], \tag{1}$$

where q_k denotes the displacement of the k-th particle from its equilibrium position and p_k its momentum. The mass μ is set to be unity. The potential takes the DW type

$$V(\xi) = -\xi^2/2 + \xi^4/4. \tag{2}$$

Such a system is very peculiar. First, equation (2) is an extension of Fermi-Pasta-Ulam (FPU) interactions to the particular DW type, which is usually adopted to model the structural phase transition [29]. Interestingly, some recent works have suggested that in the trapped-ion chains, heat transport can be feasibly tuned across the structural phase transition [30]. We have plotted the order parameter $|\langle q_{k+1} - q_k \rangle|$, the absolute values of the ensemble average of adjacent particles relative displacement (from their equilibrium positions), as a function of temperature T for several space size L (see figure 1) and verified that, for a potential like equation (2), regardless of L, there is a phase transition region around $T \simeq 0.02$-0.1. Second, we would like to note that this system does not bear linear-wave dynamics (with the unusual phonon dispersion) [31], then whether the linear phonon dynamics would still apply should be further tested. We expect that such two unusual features may affect heat transport and to understand how they may is thus interesting.

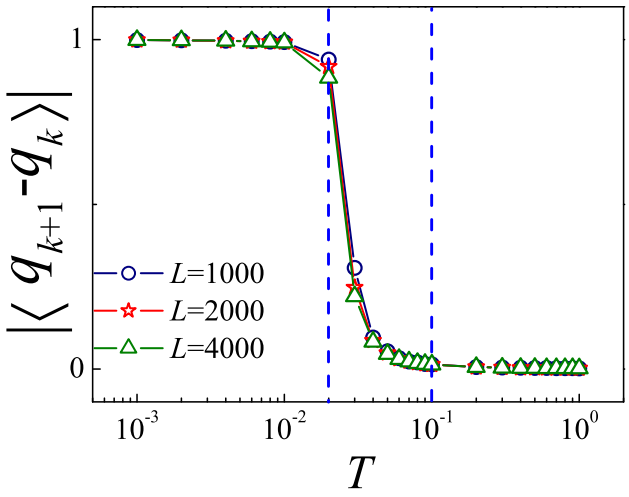

Figure 1. (Color online) The order parameter $|\langle q_{k+1} - q_k \rangle|$ vs. temperature T, where the circles, stars and triangles correspond to the results of space size $L = 1000$, 2000, 4000; and from left to right, the vertical dashed lines denote $T = 0.02$ and $T = 0.1$, respectively.

3. Simulation methods

To derive the space-time scaling for heat transport, usually one can focus on the dynamical exponent γ, defined by a space(x)-time(t) scaling analysis of the system's heat spreading density $\rho(x,t)$, i.e., $t^{-1/\gamma}\rho(t^{-1/\gamma}x,t)$. This scaling exponent has been well predicted to follow several universality classes by a recent celebrated theory of nonlinear fluctuating hydrodynamics [32, 33, 34, 35]. For a particular 1D system with conserved momentum and even symmetric potential, $\gamma = 3/2$ is suggested. From the Lévy walks theory [36], we may also have a formula $\alpha = 2 - \gamma$ that relates γ to the space scaling exponent α. Therefore, besides α, γ can also be employed to characterize the heat transport behavior, which however could provide a more detailed information.

We here aim at identifying γ from a direct dynamics simulation. For such purpose, one can investigate the decay of energy pulses or the equilibrium energy fluctuations correlation [37, 38, 39, 40, 41, 42, 43]. However, studying the energy pluses decay may be unable to avoid huge statistical fluctuations [36], hence, here we apply the equilibrium correlation method for our investigations. This correlation approach was first proposed by Zhao [39] for studying the total energy fluctuations spread and then extended to be applicable to investigate both heat and other physical quantities fluctuations decay [43]. For further detailed implementation, one can also refer to [44].

We shall mainly focus on the following three normalized spatiotemporal correlation functions of the three main physical quantities fluctuations, i.e., the heat energy, the

total energy and the momentum, defined as follows [39, 43]

$$\rho_Q(x,t) = \frac{\langle \Delta Q_j(t) \Delta Q_i(0) \rangle}{\langle \Delta Q_i(0) \Delta Q_i(0) \rangle}; \tag{3}$$

$$\rho_E(x,t) = \frac{\langle \Delta E_j(t) \Delta E_i(0) \rangle}{\langle \Delta E_i(0) \Delta E_i(0) \rangle}; \tag{4}$$

$$\rho_p(x,t) = \frac{\langle \Delta p_j(t) \Delta p_i(0) \rangle}{\langle \Delta p_i(0) \Delta p_i(0) \rangle}, \tag{5}$$

where $\langle \cdot \rangle$ represents the spatiotemporal average; $\Delta Q_i(t) \equiv Q_i(t) - \langle Q_i \rangle$, $\Delta E_i(t) \equiv E_i(t) - \langle E_i \rangle$, $\Delta p_i(t) \equiv p_i(t) - \langle p_i \rangle$ are the corresponding fluctuations; $Q_i(t) \equiv \sum Q(x,t)$, $E_i(t) \equiv \sum E(x,t)$ and $p_i(t) \equiv \sum p(x,t)$ denote the heat energy, the total energy and the momentum densities in an equal and appropriate lattice bin i (the number of particles in the i-th bin is equal to $N_i = L/b$, where b is the total number of the bins). For any particle in each bin, $E(x,t)$ and $p(x,t)$ are the single-particle's total energy and momentum at the absolute displacement x and time t; $Q(x,t) \equiv E(x,t) - \frac{(\langle E \rangle + \langle F \rangle) M(x,t)}{\langle M \rangle}$ [45] is the particle's heat energy, with $M(x,t)$ the corresponding mass density function, $\langle E \rangle$ ($\langle M \rangle$) and $\langle F \rangle$ the spatiotemporally averaged energy (mass) density and the internal pressure of the system in equilibrium state, respectively.

Note that from the definition of $Q(x,t)$, it cannot be described as a function of the lattice site, hence in practice we should have to discretize the space into several bins, thus the space variable should be the absolute displacement x rather than the label k of the particle. We emphasize that the density of $\rho_Q(x,t)$ obtained from such a key coarse-grained procedure has been verified to be more directly related to heat transport than the usually considered site-site correlation of the total energy fluctuations [43, 46].

The correlation functions $\rho_Q(x,t)$, $\rho_E(x,t)$ and $\rho_p(x,t)$ are employed to characterize the corresponding spatiotemporal spreading processes of the initial physical quantities fluctuations. If they have been obtained, then a scaling analysis may enable us to identify the corresponding transport manners.

As to our simulations, we assume the number of particles equal to the space size L, then in view of the symmetric potential of the system, the averaged pressure $\langle F \rangle$ is fixed at zero throughout the simulations. We mainly consider two cases of space size $L = 2000$ and 4000, which enables us to obtain an effective space size (about $L_{\text{effctive}} = 500 - 1000$) for a long time up to $t = 200 - 600$ for the spread. For each L, we apply the periodic boundary conditions, fix the bins number $b \equiv L/2$, and set the lattice constant $a \equiv 1$ (the choice of a has been verified not to affect the final results). We utilize the stochastic Langevin heat baths [1, 2] to thermalize the system for preparing the canonical equilibrium systems (with fixed T) and employ the Runge-Kutta algorithm of 7th to 8th order with a time step 0.05 to evolve the system. The equilibrium systems are prepared by evolving the systems for a long enough time ($> 10^7$ time units of the models) from properly assigned initial random states, then all the systems are evolved in isolation for deriving the correlation information. The size of the ensemble for deriving the correlations is about 8×10^9.

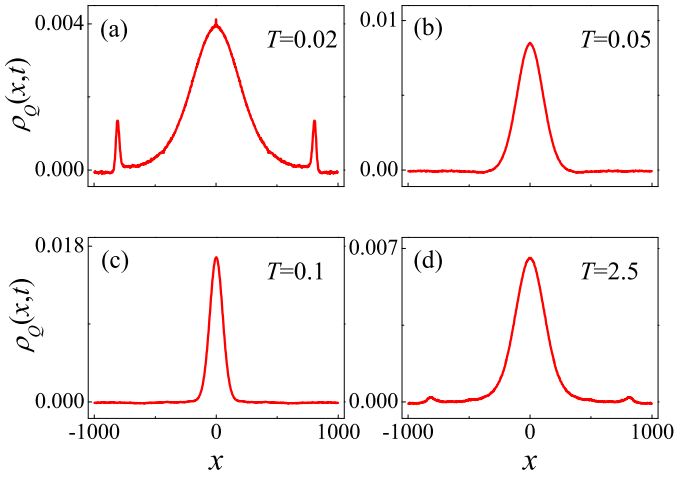

Figure 2. (Color online) $\rho_Q(x,t)$ for time $t = 600$ ($L_{\text{effective}} = 2000$) under temperatures $T = 0.02$ (a); $T = 0.05$ (b); $T = 0.1$ (c) and $T = 2.5$ (d), respectively.

4. Results

4.1. Heat transport

Now let us first see the results of heat spread. Figure 2 depicts the profiles of $\rho_Q(x,t)$ at a typical long time $t = 600$ for four temperatures, from low to high. In view of the transition region shown in figure 1, the lowest temperature considered (throughout the paper) is fixed at $T = 0.02$, up to which we have verified that the final results are insensitive to the initial states assigned to just one of the potential wells; or between the two wells alternately, or randomly. From figure 2 it can be clearly seen that the shapes of the profiles under different temperatures are different: while for a low temperature $T = 0.02$ and a high temperature $T = 2.5$ one can identify one central peak and two side peaks; in some intermediate temperature ranges, such as $T = 0.05$ and $T = 0.1$, the side peaks seem to disappear. Thus, the latter cases of $T = 0.05$ and $T = 0.1$ look like Gaussian distributions that are usually exhibited in normal transport; while for the cases that the side peaks do not disappear, $\rho_Q(x,t)$ are in good coincidence with Lévy walks stable distributions for describing superdiffusive transport [36].

Viewing this coincidence, we then perform a space-time scaling analysis for the profiles central part

$$\rho_Q(x,t) \simeq \frac{1}{t^{1/\gamma}} \rho_Q(\frac{x}{t^{1/\gamma}}, t), \tag{6}$$

which then enables us to identify a dynamical scaling exponent γ for precisely characterizing the heat transport process. We recall that usually $\gamma = 1$, $1 < \gamma < 2$ and $\gamma = 2$ correspond to the ballistic, superdiffusive, and normal transport, respectively; and in particular, $\gamma = 3/2$ is predicted by nonlinear fluctuating hydrodynamics [32, 33, 34, 35] for systems with symmetric potentials; $\gamma = 5/3$ is found by both Lévy walks approach and some numerical simulations [36, 37, 38].

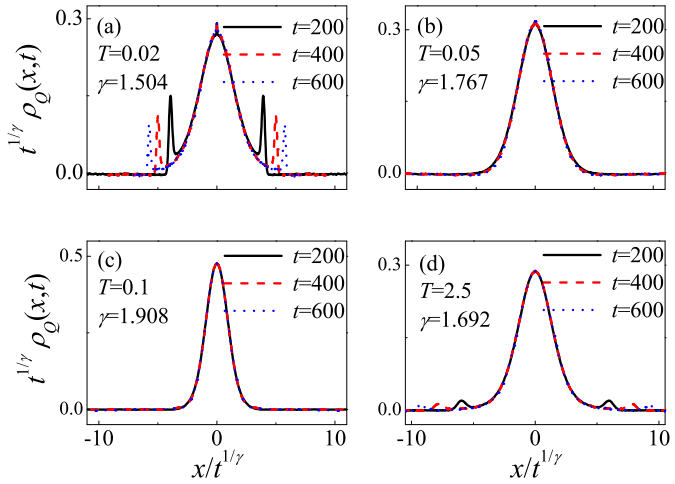

Figure 3. (Color online) Rescaled $\rho_Q(x,t)$ shown in figure 2: (a) $T = 0.02$ ($\gamma = 1.504$); (b) $T = 0.05$ ($\gamma = 1.767$); (c) $T = 0.1$ ($\gamma = 1.908$); and (d) $T = 2.5$ ($\gamma = 1.692$), respectively. In each curve scaling $t^{1/\gamma}\rho(x,t)$ vs. $x/t^{1/\gamma}$ for three different times are compared.

After obtaining the scaling exponent from formula (6), in figure 3 we plot the rescaled $\rho_Q(x,t)$ for four typical temperatures considered in figure 2. As can be seen, for all of the temperatures, formula (6) is beautifully satisfied suggesting that the focused system's heat spread can be well captured by the single-particle's Lévy walk models; though the scaling exponent γ is different for different temperatures: (i) for the lowest temperature $T = 0.02$, $\gamma \simeq 1.504$, in good agreement with the prediction $\gamma = 3/2$ of nonlinear fluctuating hydrodynamics for even symmetric potentials [32, 33, 34, 35]; (ii) in the case of high temperature $T = 2.5$, the best fitting gives $\gamma \simeq 1.692$, consistent well with the popular numerical results of $\gamma = 5/3$ based on the Lévy walks models [36, 37, 38, 40, 41, 42]; (iii) while in the intermediate ranges of temperature, γ tends to increase; in particular, around $T \simeq 0.1$, $\gamma \simeq 1.908$, suggesting that a heat transport process very close to normal ($\gamma = 2$) diffusion appears to take place, which coincides well with the early numerical findings of normal heat conduction ($\alpha \simeq 0$) in this temperature regimes [1, 19, 24].

Then what are the pictures for other temperatures? To answer this question, we carefully examine the results of $\gamma(T)$ and summarize them in figure 4. Therein four data points are extracted from figure 3, while others are calculated (fitted) additionally in the same way. For each T, two long effective space size of $L_{\text{effective}} = 1000$ and 2000 have been considered for the analysis of finite size effects. From figure 4 one can see that regardless of L, as T increases from $T = 0.02$ to $T = 2.5$, γ increases first from $\gamma \simeq 3/2$, reaches its maximum value close to $\gamma = 2$ at $T_{\text{tr}} \simeq 0.1$, then decreases down to $\gamma \simeq 5/3$ for $T = 2.5$. Thus, γ appears not a universal constant for DW systems, independence of T, and a crossover from superdiffusive ($1 < \gamma < 2$) to normal transport ($\gamma = 2$) at about $T_{\text{tr}} \simeq 0.1$ is likely to take place, though longer space sizes simulations

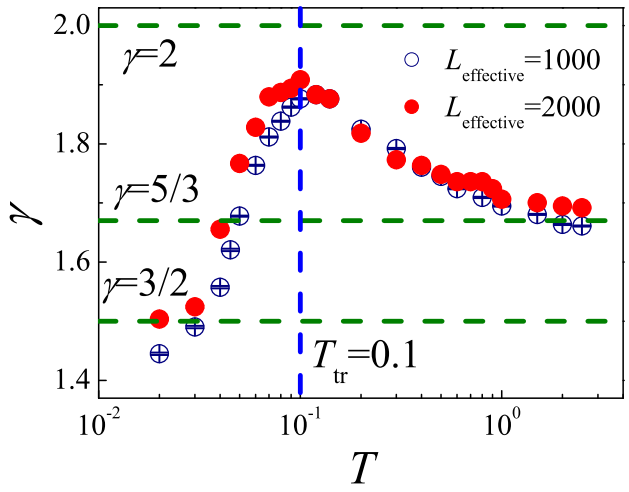

Figure 4. (Color online) γ vs. T, where the hollow (solid) circle corresponds to $L_{\rm effective}$ = 1000 (2000), and the horizontal dashed lines, from bottom to top, denote $\gamma = 3/2$, $\gamma = 5/3$ and $\gamma = 2$; the vertical dashed line denotes $T_{\rm tr} = 0.1$, respectively.

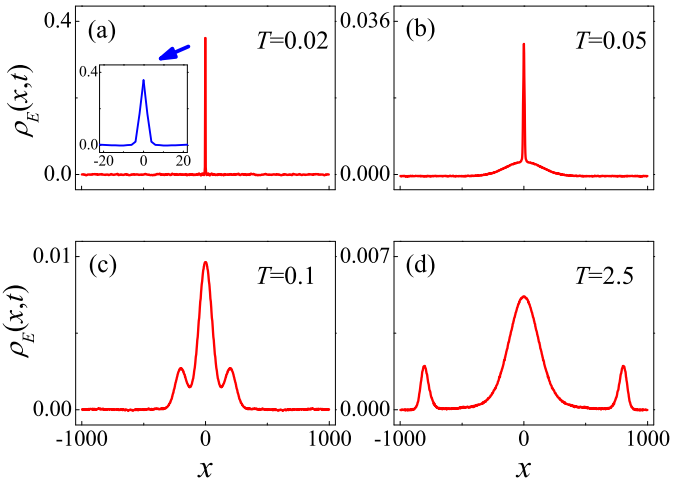

Figure 5. (Color online) $\rho_E(x,t)$ for time $t = 600$ ($L_{\rm effective} = 2000$) under system temperatures $T = 0.02$ (a); $T = 0.05$ (b); $T = 0.1$ (c) and $T = 2.5$ (d), respectively.

are still required to confirm the transition. This result is consistent with the results of α reported in [24], but obviously more precise and detailed.

4.2. Transport of total energy

Next, we turn to the results of the total energy spread. Our focus will be limited to demonstrating the distinctions between the total energy diffusion and heat spread. We will show that the spreading processes of these two physical quantities could be

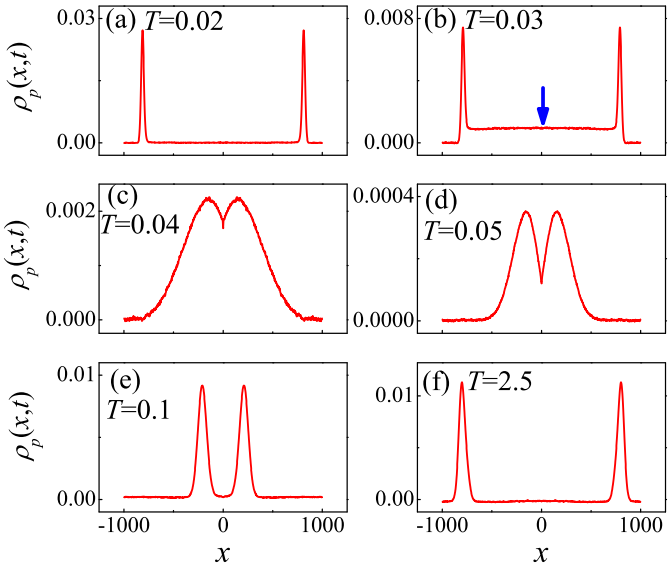

Figure 6. (Color online) $\rho_p(x,t)$ for time $t = 600$ ($L_{\text{effective}} = 2000$) under system temperatures $T = 0.02$ (a); $T = 0.03$ (b); $T = 0.04$ (c); $T = 0.05$ (d); $T = 0.1$ (e); and $T = 2.5$ (f), respectively.

very different, thus one should take very care to relate heat conduction to just energy diffusion [47].

Figure 5 shows $\rho_E(x,t)$ for four temperatures, the same as those considered in figure 2, which then enables us to make a quick comparison of the heat and the total energy spread. From figure 5 it can be seen that, despite that in the high temperatures, $\rho_E(x,t)$ shows one central peak and two side peaks as well [see figure 5(d)], similarly to $\rho_Q(x,t)$; for the cases of low temperatures, $\rho_E(x,t)$ implies very strong localizations [see figure 5(a)]; while around the crossover temperature point of $T \simeq 0.1$, there is a transition from localization to delocalization for energy [see figure 5(b)-(c)]. This phenomenon is very strange, since under some temperature regimes, the total energy is strongly localized, while heat can be superdiffusive [see figure 2(a)], the mechanisms are thus interesting and we wish to understand via further studies.

Finally, we would like to note that though the difference between $\rho_Q(x,t)$ and $\rho_E(x,t)$ is slight in the frequently considered FPU-β systems (under certain appropriate temperature regimes) [43], and there previous attempt to relate heat conduction to just the total energy diffusion in fact does not deviate too much; however, in the case of 1D DW systems considered here, concerning the heat spread obviously seems more reasonable.

4.3. Momentum transport

In order to further explore the mechanisms of normal heat transport, we then move on to the spreading process of the third physical quantity, the momentum, since a quite recent work has attributed the normal heat transport to the diffusive behavior of momentum

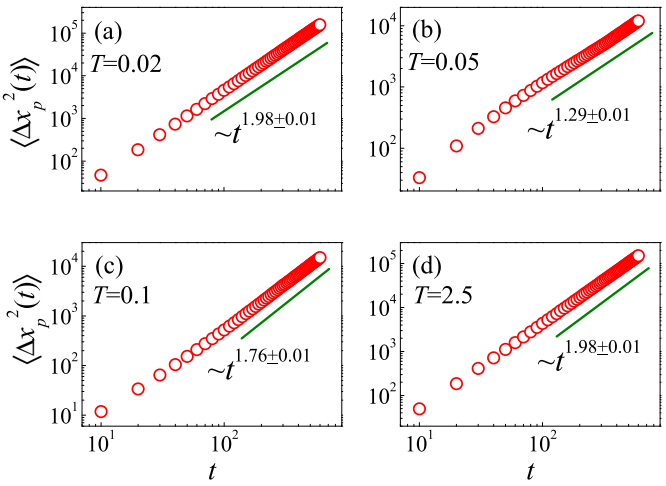

Figure 7. (Color online) $\langle \Delta x_p^2(t) \rangle$ of momentum spread vs. t for temperatures $T = 0.02$ ($\mu = 1.98 \pm 0.01$) (a); $T = 0.05$ ($\mu = 1.29 \pm 0.01$) (b); $T = 0.1$ ($\mu = 1.76 \pm 0.01$) (c), and $T = 2.5$ ($\mu = 1.98 \pm 0.01$) (d), respectively.

spread [21].

Figure 6 depicts $\rho_p(x,t)$ at time $t = 600$ for six temperatures, among which, four of them, i.e., $T = 0.02$, $T = 0.05$, $T = 0.1$ and $T = 2.5$ are those considered in figures 2-3 and 5, while two additional temperatures $T = 0.03$ and $T = 0.04$ are added for further demonstrating the details of transition. From figure 6 it can be seen that, in both cases of low and high temperatures, there are ballistic type spreading of momentum [see figure 6(a) and (f)]; however, in the intermediate temperature ranges, the non-ballistic, non-Gaussian behaviors can be clearly identified [see figure 6(b)-(e)].

The feature of momentum spread might be characterized by:

$$\langle \Delta x_p^2(t) \rangle = \sum_x x^2 \rho_p(x,t) \sim t^{\mu}, \tag{7}$$

where $\langle \Delta x_p^2(t) \rangle$ is the mean squared deviation (MSD) of momentum spread, μ is its time scaling exponent. Then $\mu = 2$ corresponds to ballistic spreading of momentum; while for $\mu = 1$, $\rho_p(x,t)$ may turn to a Gaussian distribution, thus implying a diffusive behavior of momentum spread, which has been conjectured to be related directly to the normal heat transport in the 1D rotator system [21]. Finally, $1 < \mu < 2$ then lies somewhere in between, suggesting the superdiffusive behavior.

Figure 7 presents some typical results of the MSD $\langle \Delta x_p^2(t) \rangle$ vs. t (log-log), a linear fitting then gives the scaling exponent μ. Indeed, in both cases of $T = 0.02$ and $T = 2.5$, our best fittings suggest that μ are very close to 2, thus supporting the ballistic spreading process of momentum; while for $T = 0.05$ and $T = 0.1$, the best fittings show $\mu \simeq 1.29$ and $\mu \simeq 1.76$, implying the non-ballistic, non-Gaussian superdiffusive behavior. Now it is clear that if the momentum spread with different μ can actually be related to heat transport, then the μ of $T = 0.05$ obviously shows less value than that of $T = 0.1$.

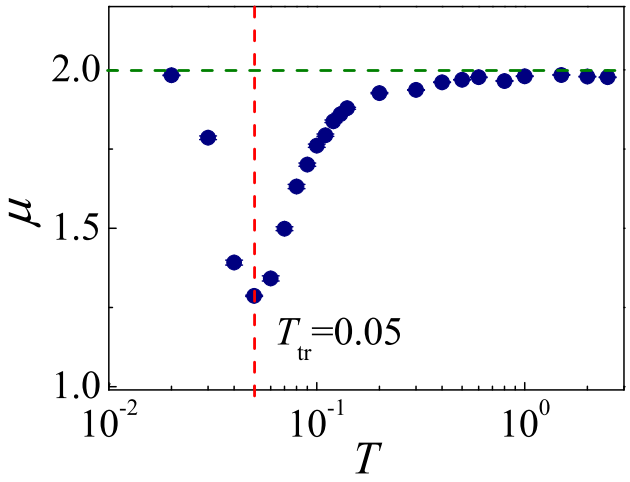

Figure 8. (Color online) Scaling exponent μ of momentum spread vs. T, where the vertical (horizontal) line denotes $T_{\rm tr} = 0.05$ ($\mu = 2$).

We thus further examine μ as a function of T and summarize the result in figure 8. As expected, a crossover from ballistic to non-ballistic momentum spread is appearing to take place; while it is $T_{\rm tr} = 0.05$, rather than $T_{\rm tr} = 0.1$ being the turning point. Unfortunately, this turning point of momentum spread seems not directly related to the crossover point of $T_{\rm tr} = 0.1$ found in normal transport of heat, though it may play a role.

In fact, such an unusual feature of momentum spread can also be detected from other measurements. For example, it is interesting to reveal the scaling properties of the peaks shown in $\rho_p(x,t)$. For such purpose one may examine how the height h of the peaks decays with time t. Since it is reasonable to assume that the peaks of $\rho_p(x,t)$ keep their volumes unchanged over the time, such an examination actually enables us to explore the dispersion of the peaks and so gain the information of sound attenuation. We have verified that the height h will scale with t as $t^{-\lambda}$ [43] in the considered long time, so here we just plot the exponent λ as a function of temperature T in figure 9. As can be seen, the result also suggests the turning point of $T_{\rm tr} = 0.05$, coincident well with the measurement of μ. Another detail is that in the high temperature regimes, the exponent λ seems to finally converge to $\lambda = 0.5$, which just gives the previous numerical findings of the exponent in the FPU-β chains [43].

It is also interesting to measure the velocity v of the peaks (which is usually suggested to correspond to the sound velocity) and compare it with the recent predictions in nonlinear fluctuating hydrodynamics [33]. Figure 10 provides such a result of v vs. T. The predictions are from the formula addressed in [33]

$$v = \sqrt{\frac{\frac{1}{2}T^2 + \langle V + \langle F\rangle \xi; V + \langle F\rangle \xi\rangle}{\frac{1}{T}\left(\langle \xi;\xi\rangle \langle V;V\rangle - \langle \xi;V\rangle^2\right) + \frac{1}{2}T\langle \xi;\xi\rangle}}, \tag{8}$$

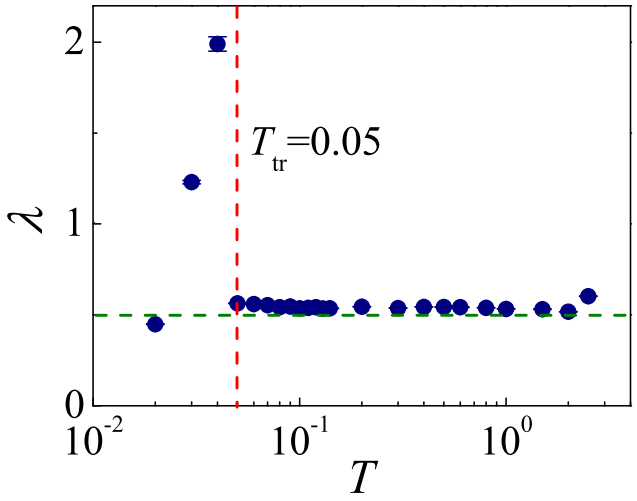

Figure 9. (Color online) Scaling exponent λ of the peaks in momentum spread vs. T, where the vertical (horizontal) line denotes $T_{\rm tr} = 0.05$ ($\lambda = 0.5$).

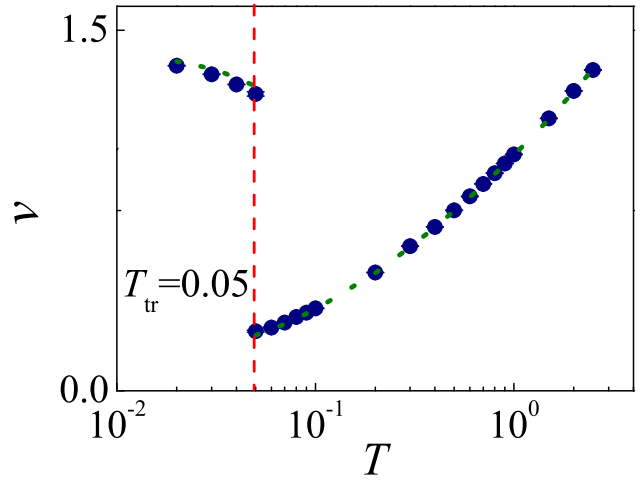

Figure 10. (Color online) The sound velocity v vs. T, where the vertical dashed line denotes $T_{\rm tr} = 0.05$; the dotted lines are the predictions from [33].

where $V(\xi)$ is the potential, $\langle A; B\rangle$ denotes the covariance $\langle AB\rangle - \langle A\rangle \langle B\rangle$ for any two quantities A and B, and $\langle F\rangle$ is the averaged pressure ($\equiv 0$ in this case). To obtain the predictions, usually one can insert the DW potential into equation (8) and calculate the ensemble average of each quantity $\langle A\rangle$ by $\int_{-\infty}^{\infty} Ae^{-V(\xi)/T}{\rm d}\xi / \int_{-\infty}^{\infty} {\rm e}^{-V(\xi)/T}{\rm d}\xi$. While for the temperatures blow the turning point of $T_{\rm tr} = 0.05$, it is reasonable to consider the integrations only over $\xi \geq 0$, i.e., $\langle A\rangle = \int_{0}^{\infty} Ae^{-V(\xi)/T}{\rm d}\xi / \int_{0}^{\infty} {\rm e}^{-V(\xi)/T}{\rm d}\xi$, since in view of the properties of the DW potential, under low temperatures, only one of the wells can be covered. So for just $T_{\rm tr} = 0.05$, we provide both predictions from different ways

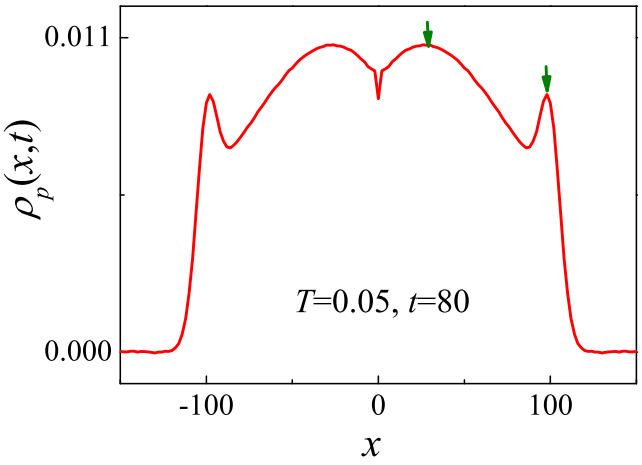

Figure 11. (Color online) $\rho_p(x,t)$ for a relative short time $t = 80$ at the turning point of temperature $T_{\rm tr} = 0.05$.

of integrations. In fact, from the simulations, around the turning point of $T_{\rm tr} = 0.05$, we can indeed identify two different ballistic peaks with different velocities in some relative short time (see figure 11). Now from figure 10, one can see that the velocities match well with the predictions, suggesting that the predictions of nonlinear fluctuating hydrodynamics can also be validated to the 1D DW systems; and more-importantly, the result clearly indicates the turning point of $T_{\rm tr} = 0.05$.

4.4. Phonons spectra

The above two crossover (turning) temperature points for heat and momentum spread naturally puzzle us. In order to better understand the mechanisms, we finally turn to analyzing how the phonons spectra $P(\omega)$ of this system would depend on temperature, from which we may gain some suggestive information.

Figure 12 depicts $P(\omega)$ vs. T for six typical temperatures considered in figure 6. For each temperature, $P(\omega)$ is calculated by applying a frequency ω analysis of the equilibrium states particles velocity $v(t)$ along the systems, i.e., $P(\omega) = \lim_{\tau\to\infty} \frac{1}{\tau}\int_0^\tau v(t)\exp(-{\rm i}\omega t){\rm d}t$. From figure 12 it can been seen that $P(\omega)$ also shows strong dependence of T, especially that in some temperature ranges, phonons tend to become "softer". These tendencies can be readily captured from the denoted peaks in the high frequency regimes.

To characterize the phonons softening and to see how it is related to thermal transport, we plot the averaged frequency $\bar{\omega}$, defined by $\bar{\omega} = \int_0^\infty P(\omega)\omega{\rm d}\omega / \int_0^\infty P(\omega){\rm d}\omega$, as a function of T in figure 13. As can be seen, besides the turning point of $T_{\rm tr} \simeq 0.1$ ($T_{\rm tr} \simeq 0.05$) for heat (momentum) spread, there is another turning point of $T_{\rm tr} \simeq 0.2$ for phonons softening. Given that $T_{\rm tr} \simeq 0.1$ just lies somewhere in between, we may conjecture that the observed normal heat transport is probably induced by the combined

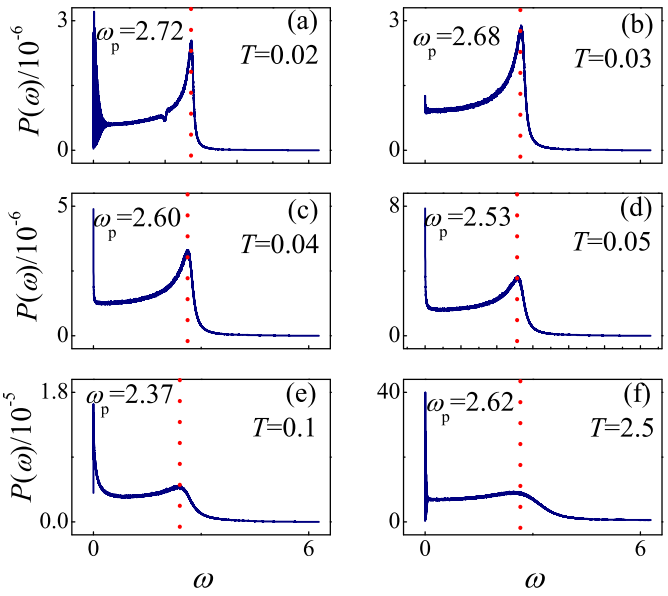

Figure 12. (Color online) Power spectra $P(\omega)$ vs. T: (a) $T = 0.02$; (b) $T = 0.03$; (c) $T = 0.04$; (d) $T = 0.05$; (e) $T = 0.1$; and (f) $T = 2.5$. The dotted lines denote the peaks with frequency ω_p in the high frequency regimes.

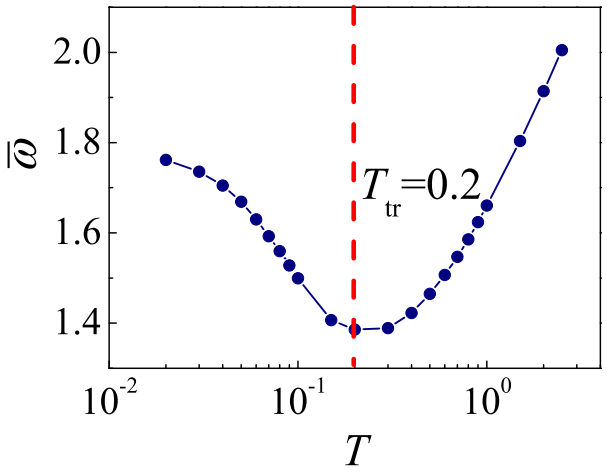

Figure 13. (Color online) The averaged frequency $\bar{\omega}$ from $P(\omega)$ vs. T, where the dashed line denotes $T_{tr} = 0.2$.

effects of phonons softening and the non-ballistic momentum spread.

About the phonon spectra calculated here, we would also like to point out that the non-ballistic behavior of momentum spread can also be detected from the phonon's lowest frequency components. We address this point by using a log-log plot of figure 12 (see figure 14). Phonons with the lowest frequency, usually called long-wavelength (goldstone) modes, are generally believed to be very weakly damped due to the conserved feature of momentum [48]. Because of their weak damping, the lowest frequency modes

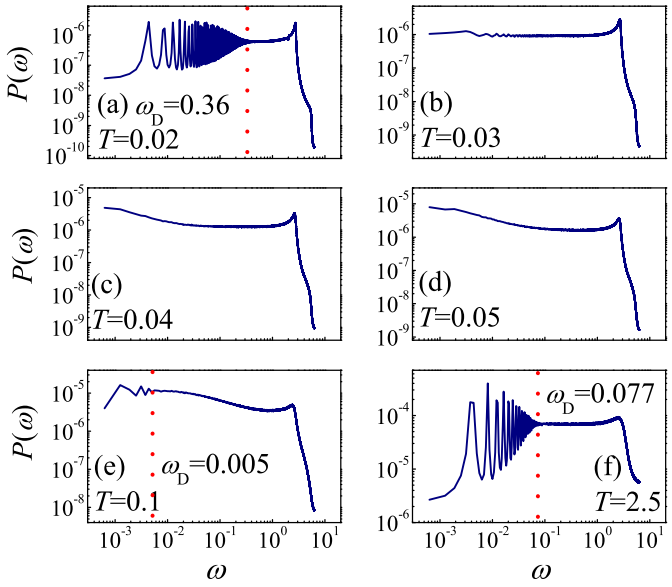

Figure 14. (Color online) Log-log plot of figure 12, where the dotted lines denote the frequencies $\omega_{\rm D}$ below which phonons are damped very weakly.

can greatly affect heat transport. From figure 14, it can be clearly seen that with the increase of T, the damping of phonons first originates from the high frequencies and then quickly walks towards the low ones. Surprisingly one may identify that a complete damping appears around the turning point of $T_{\rm tr} \simeq 0.05$ [see Figure 14(d)], the same as that found in momentum spread. This result clearly indicates a strong positive correlation between the phonons damping and the non-ballistic spreading of momentum, thus implying that the origin of the long-wavelength modes may be induced by the ballistic spreading of momentum.

5. Conclusions

To summarize, we have studied in detail the rich heat transport behaviors in the focused 1D anharmonic oscillator systems with a DW interparticle interaction like $V(\xi) = -\xi^2/2 + \xi^4/4$. By employing the equilibrium correlation method, we have captured the profiles of heat spread and precisely identified its space-time scaling exponents under various system temperatures. These heat spreading profiles are in good coincidence with the Lévy walks stable distributions, and their scaling laws show good satisfactory with Lévy walks scaling as well. Based on the scaling, we are able to present the precise temperature dependence of heat transport in this system and further verify that there is a crossover from superdiffusive to normal heat transport with a turning point at about $T_{\rm tr} \simeq 0.1$ in this particular system. This result thus provides more detailed and precise numerical evidences clearly demonstrating that normal heat transport is likely to take place in the 1D systems with DW interactions under the appropriate temperature regimes, though the total momentum is conserved here.

In order to explore the mechanisms of the observed normal heat transport, we have carefully examined the spreading of two other physical quantities, i.e., the total energy and momentum. The spreading of the total energy is found to be very distinct from heat spread. In particular, under some temperature regimes, heat can be superdiffusive, while energy shows strong localizations. This unusual result thus suggests that we should take care to derive a general connection between heat conduction and energy diffusion; rather, it may be reasonable to connect heat conduction to heat spread.

The momentum spread is shown to have a second crossover from ballistic to non-ballistic behaviors with a second turning point of $T_{\rm tr} \simeq 0.05$; however, this turning point of momentum spread cannot directly correspond to the first turning point of heat spread ($T_{\rm tr} \simeq 0.1$). So to understand the observed normal heat transport, taking only the non-ballistic behavior of momentum spread into account is inadequate. We then perform an analysis of the phonons spectra of the system. We find that phonons tend to become softest around another turning point of $T_{\rm tr} \simeq 0.2$. Together with the $T_{\rm tr} \simeq 0.05$ of momentum spread, we thus conjecture that it is the combined effects of the non-ballistic momentum spread and the phonons softening that result in the normal heat transport observed in this system. All of the simulation results seem not to contradict this conjecture, though further detailed investigations remain required.

Finally, we would like to point out that, once we have understood the mechanisms, then apart from this theoretical advance, there is also room for possible applications. For example, one may be able to vary the phonons spectrum by adjusting temperatures in other DW systems, and finally manipulate heat. Such an idea would be realized by variation of the trapping frequencies in the recent focused ion chains [49]. This kind of systems has been found to exhibit a structural phase transition similar to the DW systems [30], with which then heat transport could be tunable.

Acknowledgments

The author would like to thank the referee for his many helpful suggestions, and Profs. Hong Zhao, Jiao Wang and Yong Zhang from Xiamen university of China for their huge valuable discussions. This work was supported by the National Natural Science Foundation of China (Grants No. 11575046 and No. 11205032), the Natural Science Foundation of Fujian province, China (No. 2013J05008).

References

[1] Lepri S, Livi R and Politi A 2003 Thermal conduction in classical low-dimensional lattices *Phys. Rep.* **377** 1

[2] Dhar A 2008 Heat transport in low-dimensional systems *Adv. Phys.* **57** 457

[3] Zhong Y, Zhang Y, Wang J and Zhao H 2012 Normal heat conduction in one-dimensional momentum conserving lattices with asymmetric interactions *Phys. Rev. E* **85** 060102(R)

[4] Chen S, Wang J, Zhang Y and Zhao H 2012 Breakdown of the power-law decay prediction of the heat current correlation in one-dimensional momentum conserving lattices arXiv:1204.5933v3

[5] Savin A V and Kosevich Y A 2014 Thermal conductivity of molecular chains with asymmetric potentials of pair interactions *Phys. Rev. E* **89** 032102

[6] Das S G, Dhar A and Narayan O 2014 Heat Conduction in the α-β Fermi-Pasta-Ulam Chain *J. Stat. Phys.* **154** 204

[7] Wang L, Hu B and Li B 2013 Validity of Fourier's law in one-dimensional momentum-conserving lattices with asymmetric interparticle interactions *Phys. Rev. E* **88** 052112

[8] Chen S, Wang J, Zhang Y and Zhao H 2013 Why asymmetric interparticle interaction can result in convergent heat conductivity arXiv:1309.7146

[9] Xiong D, Wang J, Zhang Y and Zhao H 2012 Nonuniversal heat conduction of one-dimensional lattices *Phys. Rev. E* **85** 020102(R)

[10] Xiong D, Zhang Y and Zhao H 2013 Heat transport enhanced by optical phonons in one-dimensional anharmonic lattices with alternating bonds *Phys. Rev. E* **88** 052128

[11] Xiong D, Zhang Y and Zhao H 2014 Temperature dependence of heat conduction in the Fermi-Pasta-Ulam-β lattice with next-nearest-neighbor coupling *Phys. Rev. E* **90** 022117

[12] Lee-Dadswell G R, Nickel B G and Gray C G 2005 Thermal conductivity and bulk viscosity in quartic oscillator chains *Phys. Rev. E* **72** 031202

[13] Lee-Dadswell G R, Nickel B G and Gray C G 2008 Detailed examination of transport coefficients in cubic-plus-quartic oscillator chains *J. Stat. Phys.* **132** 1

[14] Lee-Dadswell G R 2015 Predicting and identifying finite-size effects in current spectra of one-dimensional oscillator chains *Phys. Rev. E* **91** 032102

[15] Popkov V, Schadschneider A, Schmidt J and Schütz G M 2015 Fibonacci family of dynamical universality classes *Proc. Natl Acad. Sci. USA* **112** 12645

[16] Hurtado P I and Garrido P L 2015 Violation of universality in anomalous Fourier's law arXiv:1506.03234v1

[17] Chang C W, Okawa D, Garcis H, Majumdar A and Zettl A 2008 Breakdown of Fouriers Law in Nanotube Thermal Conductors *Phys. Rev. Lett.* 101 075903

[18] We note that normal heat transport has also been suggested to appear in some momentum-conserving lattice or gas models close to the integrable limit, see: Chen S, Wang J, Casati G and Benenti G 2014 Nonintegrability and the Fourier heat conduction law *Phys. Rev. E* **90** 032134

[19] Giardiná C, Livi R, Politi A and Vassalli M 2000 Finite thermal conductivity in 1D Lattices *Phys. Rev. Lett.* **84** 2144

[20] Gendelman O V and Savin A V 2000 Normal Heat Conductivity of the one-dimensional lattice with periodic potential of nearest-neighbor interaction *Phys. Rev. Lett.* **84** 2381

[21] Li Y, Liu S, Li N, Hänggi P and Li B 2015 1D momentum-conserving systems: the conundrum of anomalous versus normal heat transport *New J. Phys.* **17** 043064

[22] Das S G and Dhar A 2015 Role of conserved quantities in normal heat transport in one dimenison arXiv:1411.5247v2

[23] Spohn H 2014 Fluctuating hydrodynamics for a chain of nonlinearly coupled rotators arXiv:1411.3907

[24] Roy D 2012 Crossover from Fermi-Pasta-Ulam to normal diffusive behavior in heat conduction through open anharmonic lattices *Phys. Rev. E* **86** 041102; Li H 2011 Heat conduction in one-dimensional lattice with double-well interaction *Int. Mod. Phys. B* **25** 823

[25] Xiong D 2016 Crossover between different universality classes: Scaling for thermal transport in one dimension *EPL* **113** 14002

[26] Lepri S, Livi R and Politi A 1997 Heat conduction in chains of nonlinear oscillators *Phys. Rev. Lett.* **78** 1896

[27] Narayan O and Ramaswamy S 2002 Anomalous heat conduction in one-dimensional momentum-conserving systems *Phys. Rev. Lett.* **89** 200601; Basile G, Bernardin C and Olla S 2006 Momentum conserving model with anomalous thermal conductivity in low dimensional Systems *Phys. Rev. Lett.* **96** 204303 (2006)

[28] Lebowitz J, Olla S and Stoltz G 2013 Final report of workshop "Nonequilibrium statistical mechanics: mathematical understanding and numerical simulation" http://www.birs.ca/events/2012/5-day-workshops/12w5013

[29] Schneider T and Stoll E 1975 Observation of cluster waves and their lifetime *Phys. Rev. Lett.* **35** 296

[30] Ruiz A, Alonso D, Plenio M B and Campo A del 2014 Tuning heat transport in trapped-ion chains across a structural phase transition *Phys. Rev. B* **89** 214305; Freitas N, Martínez E and Paz J P 2015 Heat transport through ion crystals *Phys. Scr.* **91** 1

[31] Lee W, Kovacic G and Cai D 2013 Generation of dispersion in nondispersive nonlinear waves in thermal equilibrium *Proc. Natl. Acad. Sci. USA* **110** 3237

[32] van Beijeren H 2012 Exact results for anomalous transport in one-fimensional Hamiltonian systems *Phys. Rev. Lett.* **108** 180601

[33] Spohn H 2014 Nonlinear fluctuating hydrodynamics for anharmonic chains *J. Stat. Phys.* **154** 1191

[34] Das S G, Dhar A, Saito K, Mendl C B and Spohn H 2014 Numerical test of hydrodynamic fluctuation theory in the Fermi-Pasta-Ulam chain *Phys. Rev. E* **90** 012124

[35] Mendl C B and Spohn H 2014 Equilibrium time-correlation functions for one-dimensional hard-point systems *Phys. Rev. E* **90** 012147

[36] Zaburdaev V, Denisov S and Llafter J 2015 Lévy walks *Rev. Mod. Phys.* **87** 483

[37] Denisov S, Klafter J and Urbakh M 2003 Dynamical heat channels *Phys. Rev. Lett.* **91** 194301

[38] Cipriani P, Denisov S and Politi A 2005 From anomalous energy diffusion to Lévy walks and heat conductivity in one-dimensional systems *Phys. Rev. Lett.* **94** 244301

[39] Zhao H 2006 Identifying diffusion processes in one-dimensional lattices in thermal equilibrium *Phys. Rev. Lett.* **96** 140602

[40] Lepri S and Politi A 2011 Density profiles in open superdiffusive systems *Phys. Rev. E* **83** 030107 (R)

[41] Dhar A, Saito K and Derrida B 2013 Exact solution of a Lévy walk model for anomalous heat transport *Phys. Rev. E* **87** 010103(R)

[42] Mendl C B and Spohn H 2013 Dynamic correlators of Fermi-Pasta-Ulam chains and nonlinear fluctuating hydrodynamics *Phys. Rev. Lett.* **111** 230601

[43] Chen S, Zhang Y, Wang J and Zhao H 2013 Diffusion of heat, energy, momentum, and mass in one-dimensional systems *Phys. Rev. E* **87** 032153

[44] Hwang H and Zhao H 2011 Methods of exploring energy diffusion in lattices with finite temperature arXiv:1106.2866v1

[45] Hansen J P and McDonald I R 2006 *Theory of Simple Liquids* 3rd ed (Academic, London)

[46] Chen S, Zhang Y, Wang J and Zhao H 2013 Connection between heat diffusion and heat conduction in one-dimensional systems *Sci. China-Phys. Mech. Astron.* **56** 1466

[47] Liu S, Xu X, Xie R, Zhang G and Li B 2012 Anomalous heat conduction and anomalous diffusion in low dimensional nanoscale systems *Eur. Phys. J. B* **85** 337

[48] Lepri S, Livi R and Politi A 2006 *Anomalous heat conduction*, a chapter of the book "Anomalous transport: foundations and applications" edited by Klages R, Radons G and Sokolov I M

[49] Häffner H, Roos C F and Blatt R 2008 Quantum computing with trapped ions *Phys. Rep.* **469** 155; Blatt R and Roos C F Quantum simulations with trapped ions *Nat. Phys.* **8** 277; Bermudez A, Bruderer M and Plenio M B 2013 Controlling and measuring quantum transport of heat in trapped-ion crystals *Phys. Rev. Lett.* **111** 040601